



Distinct bias structures for extratropical cyclones with strong or weak diabatic heating

Qidi Yu^{1,2}, Clemens Spensberger^{1,2}, Linus Magnusson³, and Thomas Spengler^{1,2}

¹Geophysical Institute, University of Bergen, Norway

²Bjerknes Centre for Climate Research, Bergen, Norway

³European Centre for Medium-Range Weather Forecasts, Reading, United Kingdom

Correspondence: Qidi Yu (qidi.yu@uib.no)

Abstract. The development of extratropical cyclones (ETCs) is often significantly altered by diabatic processes, yet the representation of these processes in numerical weather prediction models has been shown to lead to significant forecast biases. To provide a systematic quantification of 12-hour ETC forecast errors, this study uses a cyclone-centred composite framework for North Atlantic wintertime (DJF) ETCs using the ERA5 reanalysis for the period 1979 to 2022. Cyclones are categorised into 5 strong and weak diabatic heating at the time of their maximum intensification based on the domain-averaged 70th and 30th percentiles of vertically integrated diabatic heating.

While both groups exhibit a systematic underestimation of cyclone intensity, the error structures are markedly distinct. The weak heating group is characterised by an intensity underestimation near the cyclone core, whereas the strong heating group features a pronounced southwestward displacement bias together with a domain-wide intensity underestimation.

10 After removing the displacement bias, the strong heating group reveals an overestimation of low-level winds within the cold conveyor belt, sting jet, and dry intrusion regions, but a clear underestimation of moisture transport in the warm sector. These biases are accompanied by a pronounced overestimation of 850 hPa kinematic frontogenesis near the centre, likely associated with the wind field errors, and a substantial overestimation of total column liquid water along the bent-back warm front. This overestimated liquid water is likely related to the stronger frontogenesis, which induces an over-intensified secondary 15 circulation. In contrast, cyclones in the weak heating group exhibit an underestimation of wind speed and moisture near the centre, consistent with the near centre intensity underestimation. Our findings highlight the impact of diabatic heating on structural cyclone forecast biases that can guide future model improvements.

1 Introduction

Extratropical cyclones (ETCs) represent a fundamental component of mid-latitude weather, contributing substantially to the 20 global energy balance through the poleward transport of heat (Holton and Hakim, 2013) as well as being the main cause of extreme wind and precipitation events, yielding significant socio-economic losses (Pinto et al., 2012; Catto and Pfahl, 2013). The intensity and detailed structure of ETCs, particularly for extreme cases, are closely linked to diabatic processes, predominantly related to latent heat release associated with phase changes (e.g., Robertson and Smith, 1983; Vaughan et al., 2015; Joos and Forbes, 2016). Consequently, the representation of these physical processes through parameterisations in numerical weather



25 prediction (NWP) models remains a key source of systematic forecast errors and biases (Davies and Didone, 2013; Martínez-Alvarado et al., 2014b, 2016; Baumgart et al., 2018; Grams et al., 2018; Wimmer et al., 2022). Unsurprisingly, diabatic heating has thus been identified as a major contributor to forecast deficiencies for ETCs (Wernli and Gray, 2024; Sánchez et al., 2020). However, we still lack a systematic understanding how diabatic heating influences structural NWP errors for cyclones. Hence, we employ a cyclone-centred composites to contrast NWP biases and errors in ETC cases categorised by strong versus weak
30 diabatic heating.

The well-known forecast failures of severe storms, such as the QE II storm (1978) and the President's Day storm (1979), served as a wake-up call for extensive research into the role of diabatic processes in cyclone evolution (Gyakum, 1983; Bosart, 1981). Subsequent investigations rapidly established that latent heat release associated with moist processes is vital to simulate realistic cyclone development, demonstrating the capacity of latent heating to significantly intensify cyclones and fundamentally modify frontal structures (Balasubramanian and Yau, 1994; Binder et al., 2016; Joos and Forbes, 2016). Specifically, diabatic heating can modify key substructures, such as Warm Conveyor Belts (WCBs) and Cold Conveyor Belts (CCBs). While diabatic heating along WCBs can modify upper-tropospheric Potential Vorticity (PV) and thus the larger-scale flow (Wernli, 1997; Harvey et al., 2020; Oertel et al., 2020), diabatic heating in CCBs is related to the maintenance of frontal precipitation and the cloud structure in the cyclone core (Browning, 1990; Schultz, 2001; Martínez-Alvarado et al., 2014a). Furthermore, interactions between the CCB and dry intrusions (DIs) can enhance boundary-layer turbulence and evaporative cooling, thereby increasing instability on the cyclone's cold side and further modifying the CCB structure (Raveh-Rubin, 2017). Given the profound influence on both the intensity and structural details of ETCs, a systematic analysis focusing on the impact of diabatic heating on the structural representation of extratropical cyclones in NWP models is therefore essential.

Recently, forecast biases and errors in extratropical cyclones have increasingly been attributed to deficiencies in the representation of diabatic processes (Lamberson et al., 2016; Grams et al., 2018; Pickl et al., 2023). Dirren et al. (2003) diagnosed PV errors and attributed them partly to deficient diabatic processes in extratropical cyclones. Subsequently, more focused analyses have consistently shown that misrepresentation of the latent heating distribution leads to errors in upper-level PV and in the height of the WCB outflow, thereby affecting ridge building and downstream wave amplification (Teubler and Riemer, 2016; Joos and Forbes, 2016; Oertel et al., 2020). Specifically, the WCB outflow was located too far south and the associated negative PV anomaly was too weak, resulting in weak ridge amplification in the ECMWF forecasts (Martínez-Alvarado et al., 2016; Grams et al., 2018). More recently, Schäfler et al. (2024) found that diabatic process biases not only affect the ascending WCBs but also descending DIs within extratropical cyclones, leading to cold and dry biases due to underestimated surface fluxes. Despite these advances, a systematic understanding of the influence of diabatic heating on the resultant forecast errors in ETCs is still lacking.

Given the aforementioned systematic biases in ETCs forecasts, we extend the study by Yu et al. (2025) by employing a cyclone-centred composite framework to quantify short-term (12-hour) forecast biases for wintertime maritime ETCs categorised into strong and weak diabatic heating. We select the 12-hour forecast lead time, as error growth during this initial period is predominantly dominated by diabatic processes (Baumgart et al., 2019), making a comparison with the respective analysis highly effective in isolating 'fast-physics' errors in NWP models (Xie et al., 2012; Klocke and Rodwell, 2014). We fo-



60 focus on wintertime maritime ETCs, as their intensification and structural evolution are critically influenced by diabatic processes (Hoskins and Hedges, 2002; Joos and Forbes, 2016). By applying a composite approach, we provide a statistically aggregated view of how different diabatic conditions yield systematic structures in forecast biases.

2 Data and methods

2.1 Data and variables

65 We perform our analysis over the North Atlantic using the European Centre for Medium Range Weather Forecasting (ECMWF) ERA5 reanalysis for the period from 1979 to 2022 at a spatial resolution of $0.5^\circ \times 0.5^\circ$ for DJF (December, January, February) (Hersbach et al., 2020). Following Yu et al. (2025), we calculate 12-hour forecast errors using the analyses and respective 12-hour forecasts at 06 and 18 UTC. This choice is motivated by the fact that ERA5 uses forecasts initialised at 06 and 18 UTC as background (first-guess) fields in its data assimilation, ensuring close consistency between the forecasts and analyses. Such 70 consistency is desirable, as the differences between forecasts and analyses can serve as an indicator of the model's physical realism (Rodwell and Palmer, 2007).

We use mean sea level pressure (MSLP), temperature at 850 hPa, wind at 925 hPa, total column water vapour (TCWV), total column liquid water (TCLW), total column ice water (TCIW), water vapour flux (WVF), and potential vorticity (PV) as well as geopotential height at 300 hPa. In addition, we compute tangential and radial wind components at 925 hPa, as well as 75 kinematic frontogenesis at 850 hPa (e.g., Sanders and Hoskins, 1990)

$$\frac{DF_{\text{kin}}}{Dt} = \underbrace{-\frac{1}{2} |\nabla_p \theta| \left(\frac{\partial u}{\partial x} + \frac{\partial v}{\partial y} \right)}_{\text{Divergence term}} - \underbrace{\frac{1}{|\nabla_p \theta|} \left[\frac{1}{2} \left(\frac{\partial u}{\partial x} - \frac{\partial v}{\partial y} \right) \left(\left(\frac{\partial \theta}{\partial x} \right)^2 - \left(\frac{\partial \theta}{\partial y} \right)^2 \right) + \left(\frac{\partial v}{\partial x} + \frac{\partial u}{\partial y} \right) \frac{\partial \theta}{\partial x} \frac{\partial \theta}{\partial y} \right]}_{\text{Deformation term}}, \quad (1)$$

where θ is potential temperature, and (u, v) are the horizontal wind components.

2.2 Cyclone detection and tracking

ETCs are detected and tracked using the algorithm based on Murray and Simmonds (1991a, b), as implemented and refined 80 by Spensberger and Marcheggiani (2024) and Marcheggiani et al. (2025) (algorithm is publicly available as part of dynlib, Spensberger, 2024). We identify cyclones as local maxima in the Laplacian of the analysis MSLP field and track them over time using a nearest-neighbour approach combined with the most probable propagation direction. In addition, we apply several criteria to filter out non-developing and spurious systems: tracks must have a minimum lifetime of 24 hr and travel a minimum 85 distance of 500 km during their lifetime over the North Atlantic region (30° – 68° N, 80° W– 12° E). All identified cyclone centres are required to be identified as a closed system at least once within their lifetime, in line with Murray and Simmonds (1991a, b). After applying these criteria, a total of 2667 cyclone positions are retained. Our subsequent composite analysis focuses on the timestep of maximum intensification, defined as the most rapid decrease in central sea level pressure. Given that our analysis is



based on 06 or 18 UTC, we chose the analysis time closest to the timestep of maximum intensification. Other timesteps, such as genesis or maximum intensity, feature similar but weaker patterns (see Supplement Fig. S1).

90 **2.3 Compositing based on vertically integrated diabatic heating**

95 We use the diabatic temperature tendency associated with physical parameterisations, excluding radiation, to classify ETCs into strong and weak diabatic categories. We average diabatic heating at the time of maximum intensification within a radius of 750 km around the cyclone centre (similar to Tsopouridis et al., 2020) and over 700–300 hPa, where the diabatic heating tendencies are dominated by latent heating (Papritz and Spengler, 2015). Cyclones with the heating above the 70th percentile are classified as strong heating (red shading in Fig. 1a), while cyclones below the 30th percentile are classified as weak heating (blue shading in Fig. 1a). Note that maximum intensification of strong heating cyclones predominantly occurs at lower latitudes, often located around the SST front regions along the Gulf Stream, whereas weak heating cyclones occur more frequently at higher latitudes (Fig. 1b).

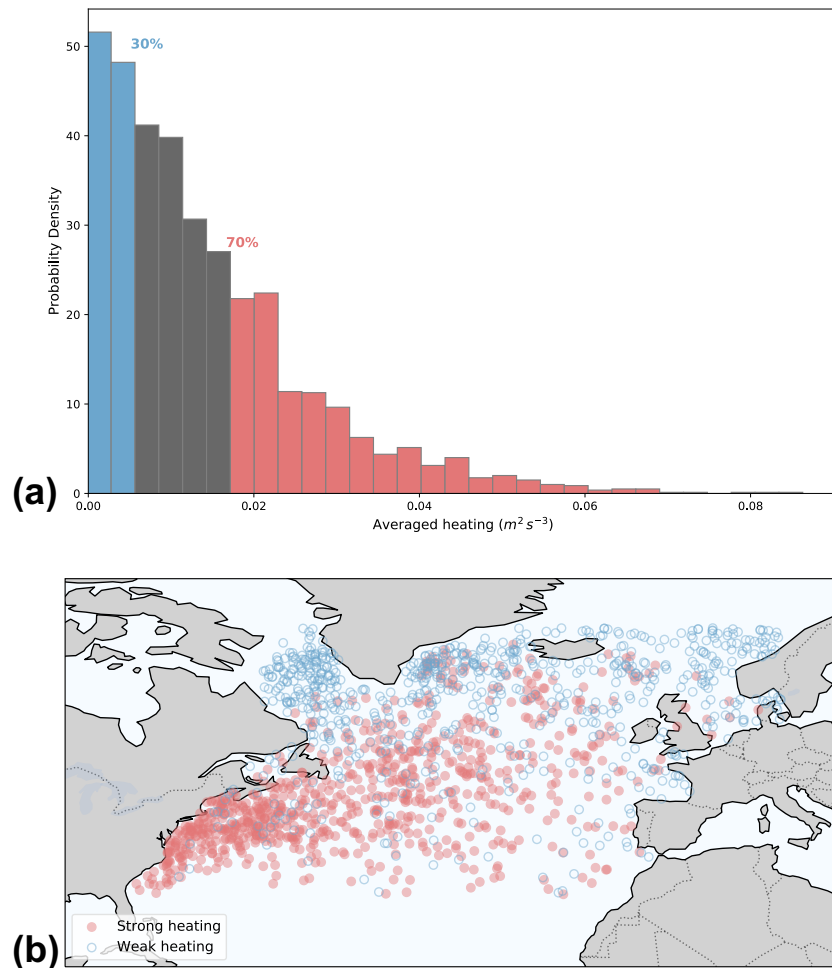


Figure 1. (a) Probability density function of the vertical integral of diabatic heating (excluding radiation) averaged over the horizontal extent of the cyclone($m^2 s^{-3}$) at maximum intensification, and (b) geographical distribution of cyclone centres for the strong and weak heating groups at maximum intensification.



We analyse cyclone forecast biases at maximum intensification using cyclone-relative composites for the two heating categories. Following (Catto et al., 2010), all fields are rotated so that motion in all composites is aligned along the x-axis, ensuring
105 that mesoscale features, such as fronts and air mass sectors, are consistently positioned in the composites.

2.4 Re-aligning cyclone centers

The thus derived composites illustrate why we chose to include one additional step in the analysis method (Fig. 2). Cyclone-centred error composites for both weak and strong heating show a systematic underestimation of intensity, with forecasted MSLP contours (blue contours) having a smaller radius compared to the analysis (black contours, Fig. 2a,b). For weak heating,
110 this intensity underestimation is also clearly depicted by the positive MSLP bias (shading, Fig. 2b) and the corresponding negative bias in the 925 hPa wind around the cyclone centre (Fig. 2 d).

For strong heating, however, the MSLP bias features a pronounced dipole pattern (Fig. 2a), attributable to a southwestward displacement of the forecasted cyclone, implying a too slow propagation of the cyclone in the forecast. This positional bias is supported by the strong dipole pattern observed in the 925 hPa wind field near the centre (Fig. 2c). The combined bias in
115 both intensity and propagation is consistent with (Froude et al., 2007), who found the ECMWF model to generally forecast too shallow and too slow cyclones in the Northern Hemisphere winter. While the forecast bias for weak heating is predominantly associated with an underestimation of intensity, a similar slight southwestward displacement is also evident.

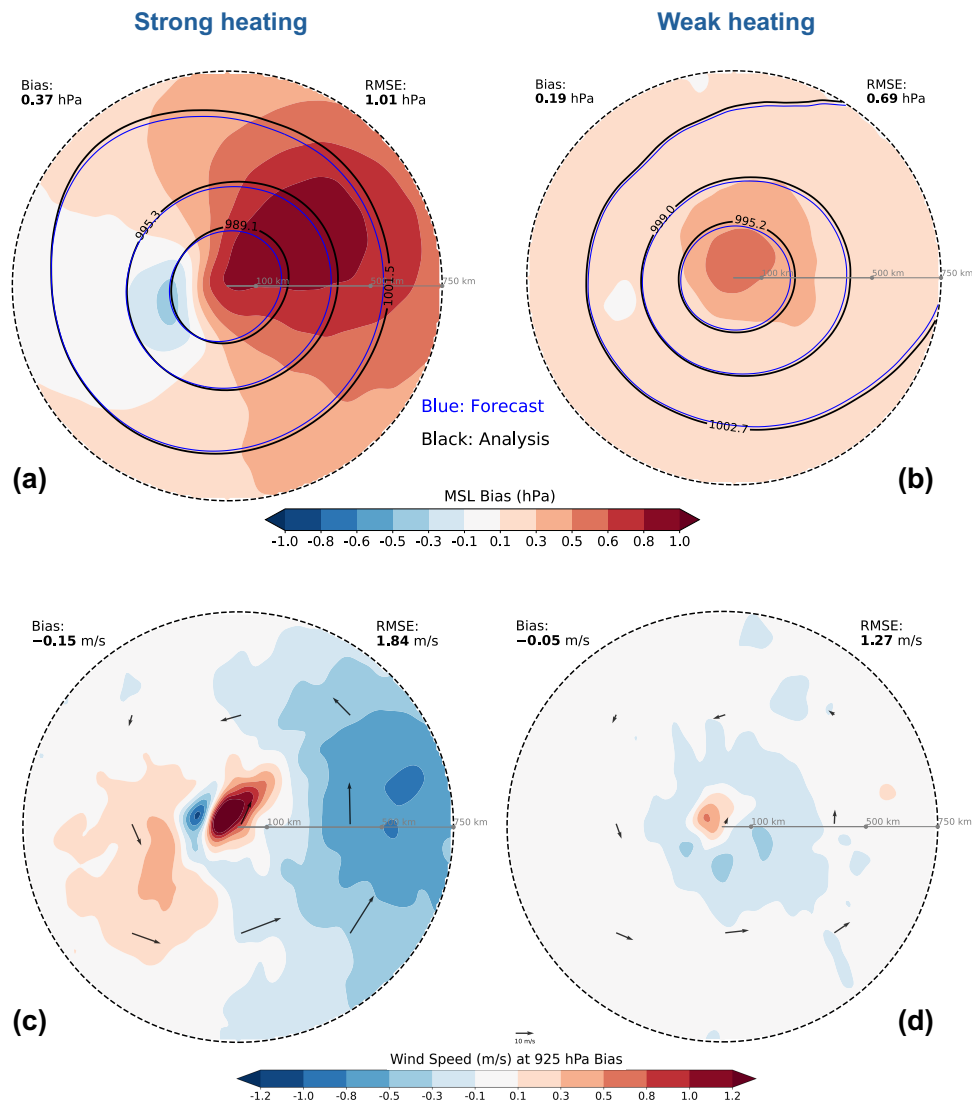


Figure 2. Biases for (a,c) strong heating group and (b,d) weak heating group: (a,b) mean sea level pressure (MSLP) (hPa) bias composite (shading), analysis composite (black contours), forecast composite (blue contours) and (c,d) wind speed bias (m/s) at 925 hPa (shading), black (blue) quivers show analysis (forecast) wind composite.



To focus on cyclone-centre-relative errors, we remove the aforementioned positional bias by redefining the respective cyclone centres in both analysis and forecast as the location of the nearest minimum in MSLP compared to the originally detected cyclone centre in the analysis. Analogous to the tracking, the MSLP field is spatially filtered using spectral triangular truncation 125 (T84). This filtering procedure effectively filters out small-scale noise. We require that the identified MSLP minima in both the analysis and forecast must be within a 250 km radius of the originally detected centre in the analysis. Any cyclone record failing this criterion is discarded.

The ‘strong’ and ‘weak’ heating groups, defined as the top and bottom 30% of the diabatic heating distribution, initially 130 comprise 801 and 799 cyclones, respectively. After this filtering and re-centring, a total of 774 and 627 analysis-forecast pairs are retained for the strong and weak heating group, respectively. We use the re-centred data for analysis and forecast to compile our cyclone-centred composite analysis. Given that both analysis and forecast are now centred on the position of minimum MSLP, the positional bias in the composites has been removed (compare Figs. 2 and 3).

3 Cyclone-centred error composites

3.1 MSLP and 925 hPa wind

135 Cyclone-centred MSLP biases reveal an underestimation of cyclone intensity, with structural differences for the two groups (Fig. 3a, b). For strong heating, a broad area with a positive bias is evident, indicating that the forecasted cyclone is too shallow (Fig. 3a, shading). This underestimation is also visible in the forecasted MSLP contours (blue), which have a smaller radius compared to the analysis (black). The weak heating group also features intensity underestimation, though restricted to the inner-core (Fig. 3b).

140 Notably, a comparison with the non-centred results (Fig. 2a, b) reveals that the recentred composites (Fig. 3a, b) exhibit a smaller domain-averaged bias but a larger domain-averaged RMSE. This counter-intuitive increase is most likely due to the elimination of error compensation, where the position bias originally masked the systemic intensity underestimation. Specifically, in the non-recentred composite (Fig. 2a, b), the southwestward displacement partially overlaps with the regions of intensity underestimation, leading to a cancellation of biases over the left-hand quadrants of the composite. Once recentred (Fig. 145 3a, b), this spatial offset is removed, revealing a more consistent and domain-wide intensity bias. While recentring reduces the large error magnitudes near the cyclone centre, broadly distributed errors lead to a higher domain-averaged RMSE.

The weak heating group displays an underestimation of 925 hPa wind around the cyclone centre (Fig. 3d), which is consistent 150 with the underestimated depression in MSLP (Fig. 3b). The strong heating group, on the other hand, exhibits a wind speed underestimation only in the warm sector, while wind speed is overestimated in the cold sector over (Fig. 3c), the region usually associated with the Cold Conveyor Belts (CCBs), dry intrusions (DIs), and sting jets (SJs) (Schultz, 2001; Browning, 1997, 2004). One potential explanation for this overestimation is that the stronger winds in the forecast may in fact be closer to the real CCB/SJ/DI wind speeds, consistent with marine CCB jets being underestimated in ERA5 (Gentile and Gray, 2023). Despite these spatial variations, both heating groups demonstrate a domain-averaged underestimation of 925 hPa wind speed, which generally aligns with previous feature-based analyses (Yu et al., 2025).

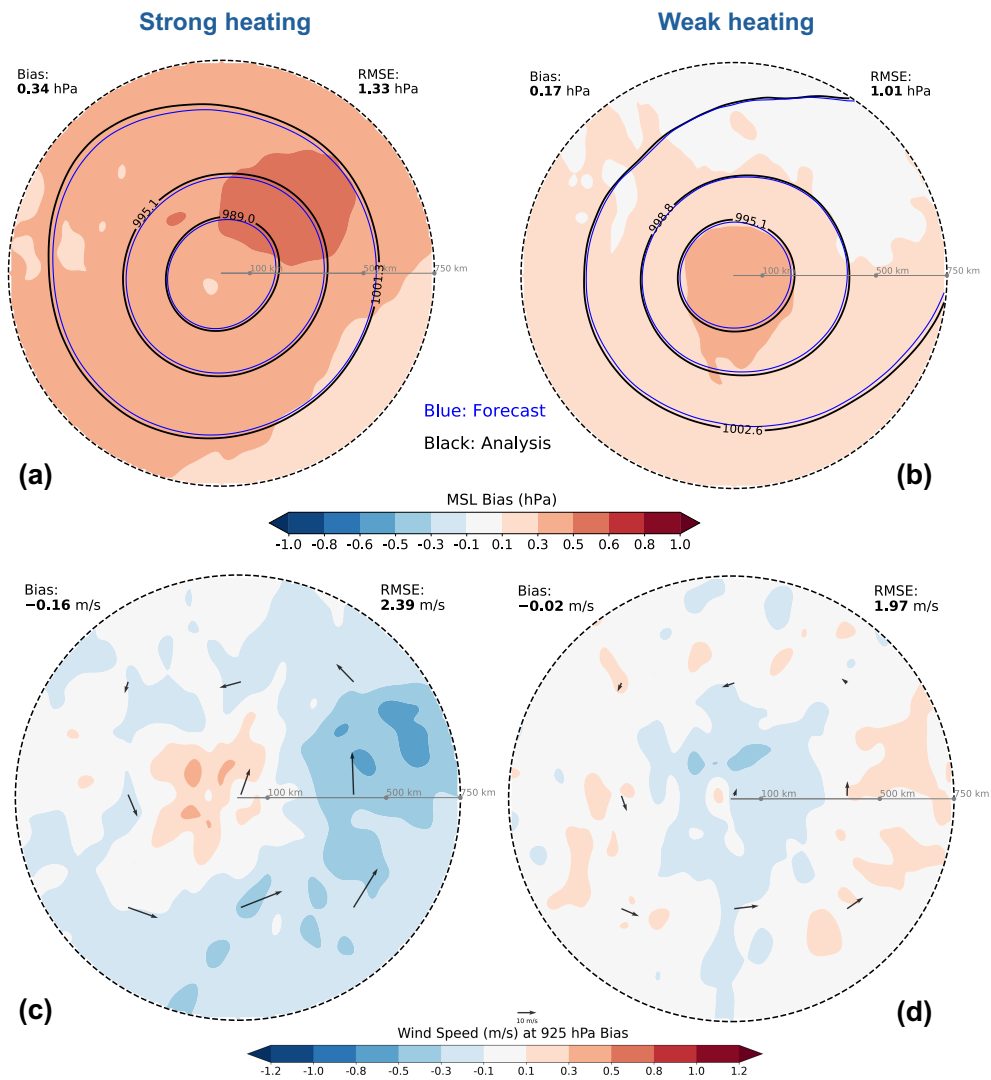


Figure 3. As in Figure 2, but after removing the position shift.



3.2 Moisture fields

For the strong heating group, the total column water vapour (TCWV) composite reveals a distinct negative bias, indicative of a moisture deficit in the forecast (Fig. 4a). This underestimation is most pronounced in the warm sector, especially along the 160 boundaries of high TCWV filament (about 4%). A comparison of the composite contours shows that the water vapour in the forecast (blue) is narrower compared to the analysis (black). In addition, a pronounced negative bias of the water vapour flux (WVF) is evident in both the along and across components relative to cyclone propagation on the warm side of the cyclone (Fig. 4e, f). The TCWV deficit is thus consistent with insufficient moisture transport in the warm sector, most likely coinciding with warm conveyor belts.

165 The high-value core of total column ice water (TCIW) is located at the upper right-hand quadrant of the composite cyclone, with its trailing region at the bottom right-hand quadrant. There is a negligible bias within the maximum of TCIW, with negative/positive biases at the leading/trailing edge of the TCIW maximum (Fig. 4b). The TCIW plume in the forecast (blue contours) is more elongated than in the analysis (black contours). This more elongated structure of the forecasted TCIW is the main cause of the positive bias in the trailing region, indicating that the ice water is less cyclonically wrapped up in the 170 forecast. This weaker wrap-up is consistent with the insufficient moisture transport and underestimated wind (Fig. 3c,d).

In contrast to the underestimation for vapour, the total column liquid water (TCLW) shows a notable positive bias (approximately 10% overestimation) within the upper two quadrants of the composite close to the cyclone centre, commonly referred to as the cloud head region. (Fig. 4c). This bias might be attributable to error sources from both microphysics and dynamics.

175 The positive TCLW bias is concentrated within the strong ascent region (Fig. 4c). Given the corresponding negative biases in TCWV, the bias in TCLW could indicate issues with the microphysical scheme, having a too low precipitation efficiency with liquid droplets remaining suspended rather than precipitating out of the atmospheric column. This issue can be exacerbated by the limitations of data assimilation (DA). As liquid water is not directly constrained by DA (Geer et al., 2017), the model must rely on indirect corrections via adjustments to thermodynamic and kinematic observations, which may feature systematic deviations, potentially yielding the positive liquid water bias.

180 Given that vertical velocity in the analysis is diagnosed and not directly observed, we employ the kinematic frontogenesis of potential temperature (θ) as a proxy, as it quantifies the dynamic forcing that drives a secondary vertical motion (Sawyer, 1956; Eliassen, 1962). Pronounced frontogenesis at 850 hPa is evident in the upper left- and right-hand quadrants of the cyclone centre (Fig. 4d). The frontogenesis positioned closer to the cyclone centre is associated with a positive bias in frontogenesis near the centre ($\sim 17\%$). Through thermal wind, the resulting enhanced temperature gradient strengthens the vertical shear of 185 the geostrophic wind, consistent with the wind speed overestimation (Fig. 3c). The intensified frontogenesis is also associated with a secondary circulation that produces enhanced vertical motion on the warm side of the front (not shown). This ascent can enhance condensation, potentially resulting in an overestimation of liquid water along the warm front (Fig. 3c), which would be consistent with Martínez-Alvarado et al. (2014b), who showed that latent heating strongly influences the frontal structure and cyclone intensity.

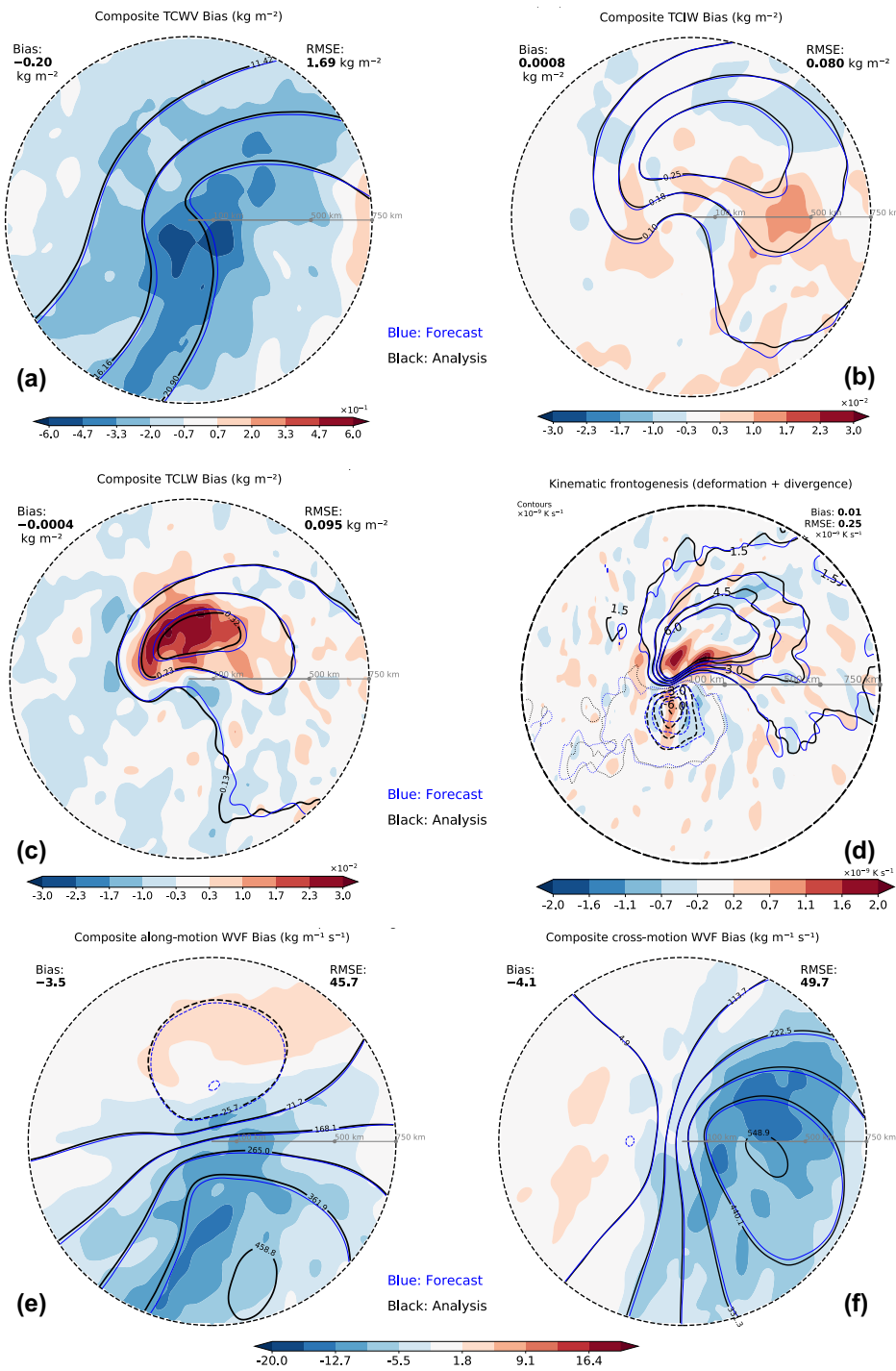


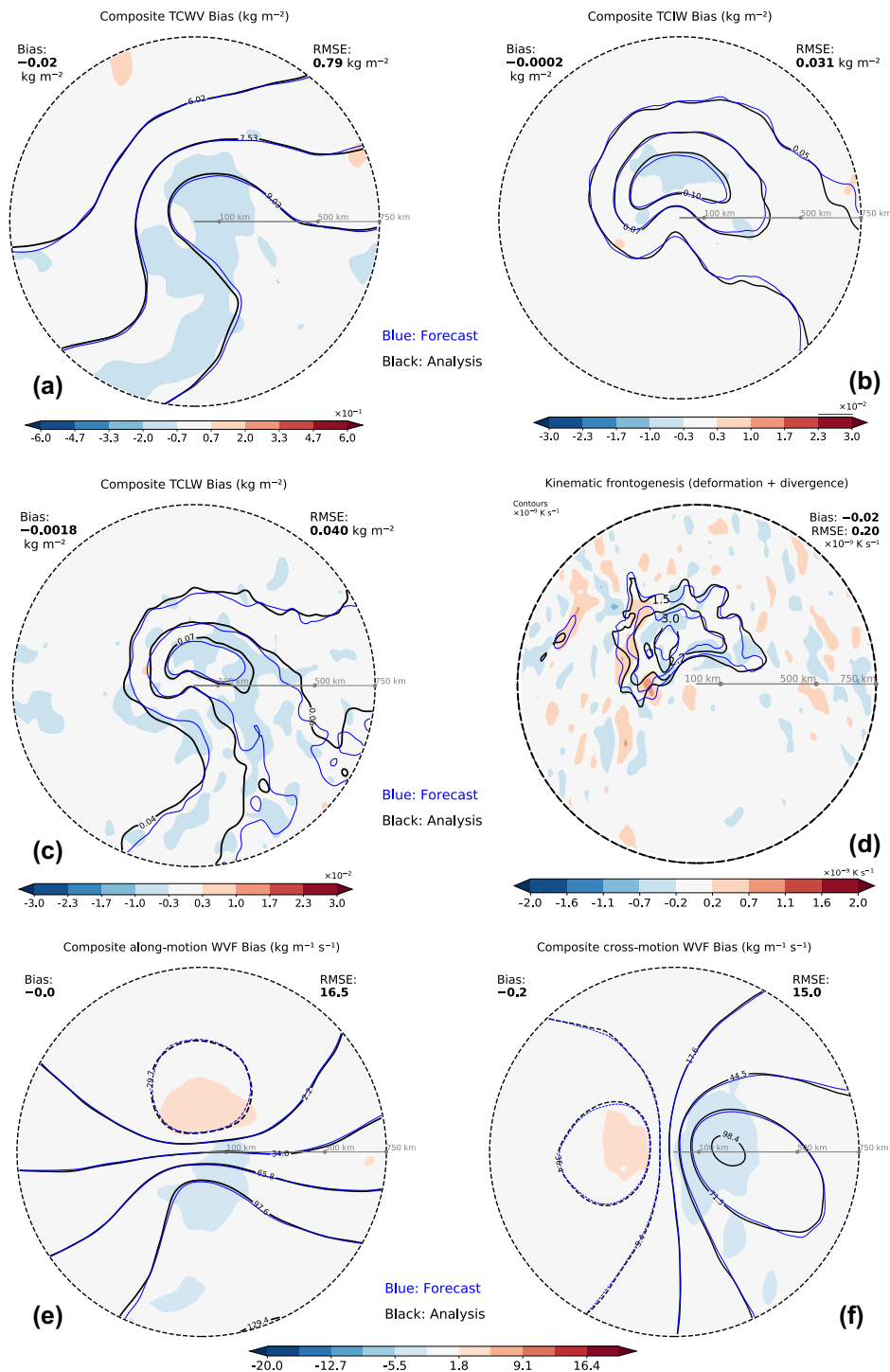
Figure 4. Biases for the strong heating group: (a) total column water vapour, (b) total column ice water, (c) total column liquid water, (d) kinematic frontogenesis, (e) along-motion water vapour flux, and (f) cross-motion water vapour flux.



Compared with the strong heating group, the weak heating group exhibits a much weaker bias of TCWV, mainly around the centre (approximately 1%) as well as on the left side of the high TCWV filament (Fig. 5a). Accordingly, moisture transport
195 also shows only very weak biases near the centre (Fig. 5e,f). The biases are smaller and exhibit a more symmetric distribution of positive and negative bias compared with the strong heating group (compare Fig. 4e,f and Fig. 5e,f). Given that these biases for the strong heating group are primarily associated with the warm sector, the weaker asymmetry and bias could also be due to weak heating cyclones occurring primarily at higher latitudes (Fig. 1b), limiting the moisture supply, resulting in less pronounced biases.

200 Both TCIW and TCLW composites also display notably smaller negative biases in the respective high-value regions ($\sim 1\%$, Fig. 5b,c). The smaller biases for both liquid and frozen water for the weak heating group is likely also related to the lower moisture availability at higher latitudes, also resulting in the reduced diabatic heating.

Consistent with the biases above, the bias in kinematic frontogenesis is also much smaller compared to the strong heating group (Fig. 5d). This primarily reflects the weaker baroclinicity and frontogenetic intensity of these higher-latitude cyclones.





3.3 Tangential and radial wind components

For cyclones with strong heating, tangential winds at 925 hPa are underestimated in the warm sector, indicating a weaker cyclonic circulation in forecasts (Fig. 6a). This is consistent with the underestimated wind at 925 hPa (Fig. 3c) as well as the 210 underestimated moisture transport (Fig. 4e,f). In contrast, tangential winds are overestimated near the cyclone centre, consistent with the wind bias around the CCB, DI, and SJ (Fig. 3c). The latter overestimation of cyclonic wind is also associated with the overestimation of frontogenesis (Fig. 4d). An accurate representation of these winds is particularly important, as the CCB region is most frequently associated with compound wind-wave hazards (Gentile and Gray, 2023), with SJs often contributing to extreme wind gusts (Clark and Gray, 2018).

215 Radial wind also features a domain-averaged positive bias, indicating an underestimation of inflow in the forecast (Fig. 6c), which is consistent with the previously reported wind direction bias for cyclones (Yu et al., 2025). Notably, a pronounced negative bias is observed in the radial wind within the upper right-hand quadrant of the composite cyclone near the centre. This negative bias indicates an overestimation of inflow (convergence), which is most likely associated with an overestimated vertical motion resulting from the frontogenesis bias (Fig. 4d).

220 The low-level tangential wind composite for cyclones with weak heating exhibits a clear underestimation near the cyclone centre (Fig. 6b). This indicates a weaker cyclonic circulation in the forecast, consistent with cyclones in this group being forecasted too weak (Fig. 3b). Correspondingly, the radial wind component generally displays a small domain-averaged positive bias (Fig. 6d). The clearest positive bias is located in the warm sector. This reflects a weaker inflow and insufficient convergence within the warm sector, which is essential for cyclonic development and warm frontal ascent.

225 3.4 Temperature at 850 hPa

The temperature bias for the strong heating group shows a pronounced cold bias in the upper right-hand quadrant. This is consistent with the underestimated cyclonic flow and water vapour transport in the warm sector, thus featuring reduced warm air advection (Figs. 3c, 4e,f, and 6a). Additionally, the lower-left quadrant also exhibits a notable cold bias. This cold bias is linked to the upper level potential vorticity (PV) biases discussed in the following section.

230 For the weak heating group, the temperature bias at 850 hPa manifests as a cold bias in the warm sector (lower-right quadrant) and a warm bias in the cold sector (upper-left quadrant, Fig. 6f). This pattern is consistent with the underestimation of cyclone intensity.

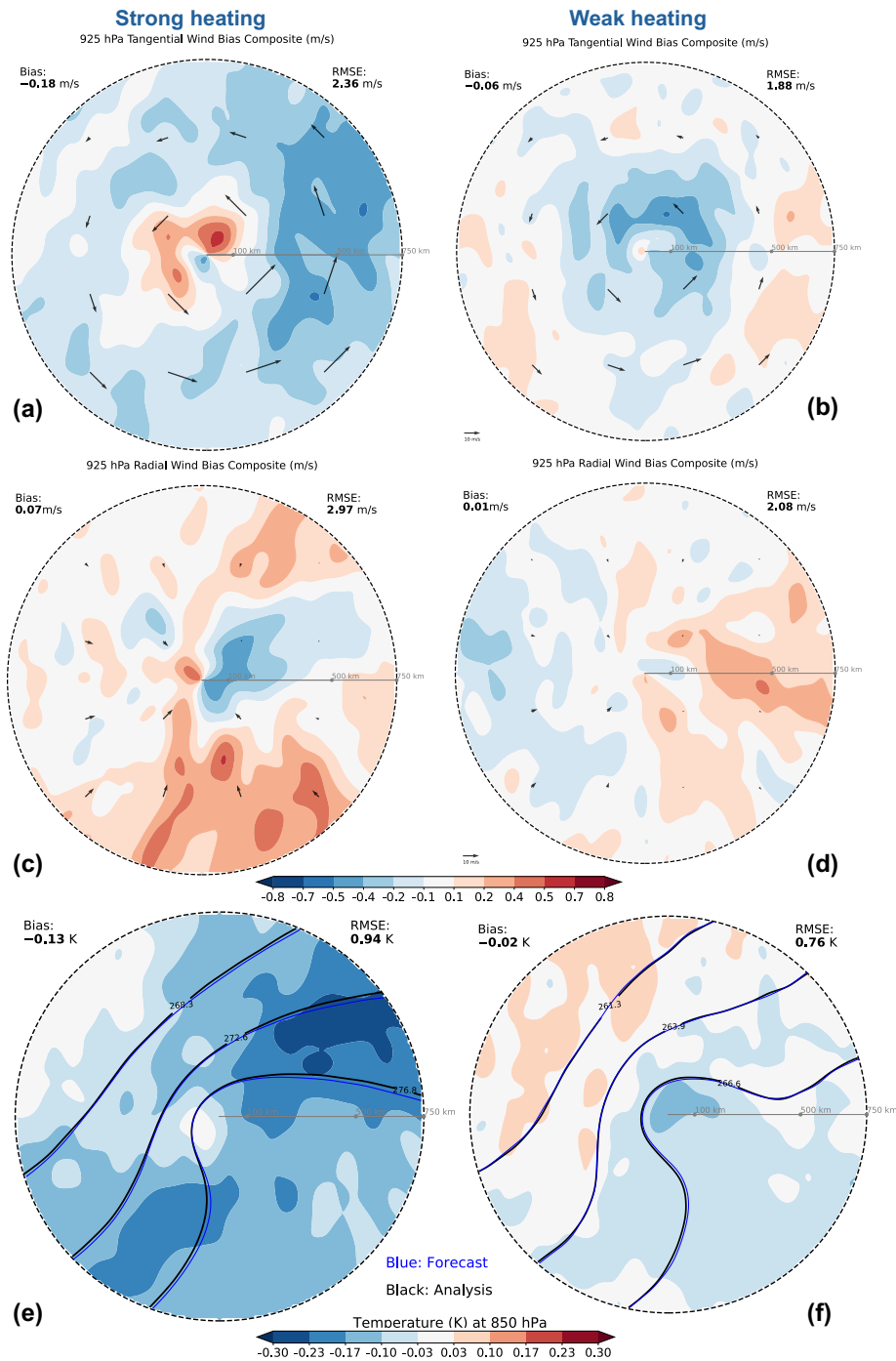


Figure 6. Biases for (a, c, e) the strong heating group and (b, d, f) the weak heating group. Panels (a, b): tangential wind bias composite at 925 hPa (shading) with analysis composite (quivers). Panels (c, d): radial wind bias at 925 hPa (shading) with analysis wind composite (quivers). Panels (e, f): temperature bias at 850 hPa (shading) with analysis/forecast composite (black/blue contours).

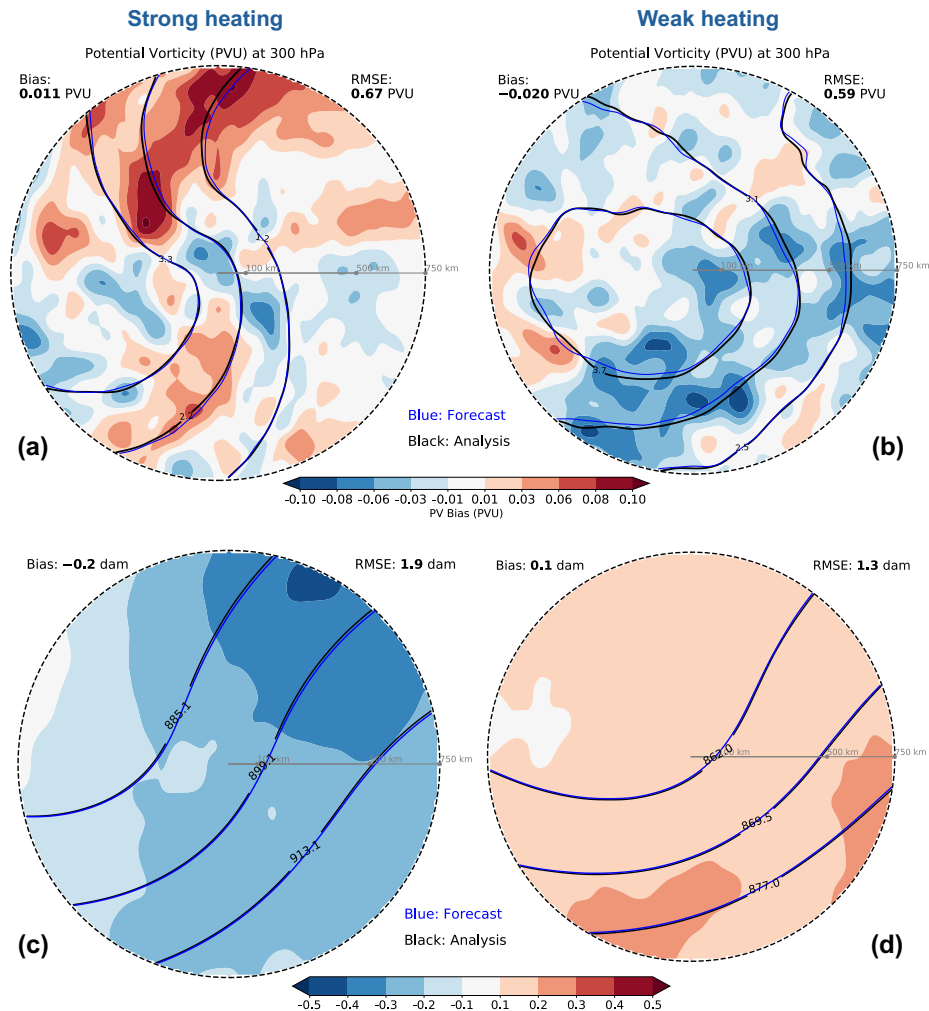


3.5 Upper-level circulation at 300 hPa

The upper-level PV field for the strong heating group displays a distinct trough-ridge pattern, with a pronounced positive bias around the ridge (Fig. 7a). This underestimation of the upper-level ridge in the presence of strong diabatic heating is consistent 240 with previous studies (Martínez-Alvarado et al., 2016; Grams et al., 2018; Oertel et al., 2020). Furthermore, although the trough axis generally exhibits an underestimation (negative bias), there is an elongated positive PV bias along the trough axis, indicating an overestimation of PV in the forecast. The positive PV bias co-locates with the cold bias in the lower-left quadrant (Fig. 6e). This overestimation of upper level PV is likely associated with enhanced descending along dry intrusions (DI), which can result in larger cold and dry air advection within the cold sector (Catto and Raveh-Rubin, 2019).

245 Consistent with the upper level PV bias, the bias in geopotential height at 300 hPa for cyclones with strong heating features an underestimation of the ridge (Fig. 7c). Note, however, that the trough is not underestimated in terms of geopotential. The underestimations of both the upper-level PV and geopotential are most likely due to misrepresentations in diabatic heating and are thus consistent with biases presented earlier, such as the underestimation in water vapour transport (Figs. 4a,e,f), wind (Fig. 3c, 6a), and temperature (Fig. 6e). Overall, these biases are most likely linked to an underestimated strength of the WCB. 250 Our findings are thus consistent with previous studies showing that an underestimation in WCB intensity results in a weaker negative PV anomaly and thus a weaker upper-level ridge (Martínez-Alvarado et al., 2016; Grams et al., 2018; Harvey et al., 2020; Oertel et al., 2020).

The PV composite for the weak heating group shows a maximum in PV above the cyclone centre, with contours extending upstream (Fig. 7a). The bias generally features an underestimation of upper-tropospheric PV, consistent with a weaker cyclone 255 in terms of MSLP (Fig. 3b). In contrast to the strong heating group, the geopotential height field in the weak heating group generally shows a spatially uniform positive bias (Fig. 7d), consistent with the PV trough being underestimated, as well as underestimation of cyclone intensity (Fig. 3b).



260 **Figure 7.** Biases for (a, c) the strong heating group and (b, d) the weak heating group. Panels (a, b): potential vorticity (PV) bias composite at 300 hPa (shading) with analysis composite (black contours), forecast composite (blue contours). Panels (c, d): geopotential height at 300 hPa.



4 Conclusions

This study employs a cyclone-centred composite framework to quantify short-term (12-hour) forecast biases for wintertime (DJF) maritime extratropical cyclones (ETCs) within the ERA5 for the period 1979–2022. To compare the influence of diabatic processes, cyclones are categorised into groups based on strong and weak intensity of domain-averaged diabatic heating. Overall, 12 h forecasts of North Atlantic extratropical cyclones underestimate cyclone intensity at the time of maximum intensification. However, the bias pattern for the strong and weak heating groups shows distinct differences. While, forecasts primarily underestimate cyclone intensity near the cyclone centre for the weak heating group, forecasts not only underestimate cyclone intensity, but also feature a propagation bias, manifesting as a southwestward displacement of the cyclone position, for the strong heating group.

After removing the displacement bias, the primary near-centred intensity underestimation is confirmed for the weak heating group. This is evident in the clear underestimation of low-level cyclonic flow around the cyclone centre. As well as the near-centred underestimations in TCWV, TCLW, TCIW, and WVF. Additionally, the low-level temperature field reveals a cold bias in the warm sector and a warm bias in the cold sector, indicative of a weaker horizontal temperature gradient across the system and an insufficient baroclinic development in the forecast. At the upper levels, the PV field also features a systematic underestimation, consistent with the shallower, weaker surface system.

After removing the overall positional displacement bias, the strong heating group exhibits a domain-wide positive MSLP bias, reflecting an underestimation of cyclone intensity. This underestimation manifests particularly in the warm sector, with a consistent negative biases in low-level cyclonic flow, water vapour, and water vapour transport, alongside a cold temperature bias. These negative biases go together with an underestimated moist transport within the cyclone's warm sector, potentially limiting upper-level ridge building. In contrast, strong heating cyclones feature a pronounced overestimation of total column liquid water along the bent-back warm front, a region typically characterised by intense latent heat release.

Composite 850 hPa kinematic frontogenesis reveals a more inward spatial configuration of the frontogenetic zone relative to the cyclone centre in the high-latent heating forecast than in the analysis, resulting in a pronounced overestimation of frontogenesis near the centre. This intensification of frontogenesis is likely driven by the overestimated wind speeds within the CCB/SJ/DI region, which enhance the local kinematic deformation and convergence. To maintain thermal wind balance, this strengthened frontogenesis induces an intensified secondary circulation, with enhanced ascent on the warm side of the front. The intensified ascent can lead to an increase in condensation, thereby resulting in the observed positive bias in total column liquid water. This overestimation of liquid water suggests a potential bias in precipitation efficiency, whereby liquid droplets remain suspended in the atmospheric column rather than precipitating out. This may be exacerbated by limitations of the data assimilation (DA), as liquid water is not directly constrained and the DA relies on indirect adjustments to thermodynamic and kinematic fields.

It remains an open question whether the wind speed overestimation for the CCB/SJ/DI regions in the forecasts reflects a true model bias or a systematic underestimation within the analysis. This bias may arise from the scarcity of high resolution observations over the open ocean, which limits the data assimilation system's ability to resolve localised, high-intensity



features such as the CCB and SJ. Consequently, the resulting analysis may represent a smoothed state, failing to capture the full magnitude of the wind field, thus making a potentially physically more realistic forecast appear as a positive bias. Addressing this uncertainty requires targeted observations, such as those planned for the upcoming NAWDIC (North Atlantic Waveguide and Downstream Impact Campaign Raveh-Rubin et al. (2025)), which aims to provide detailed observations. How 300 the bias in this area may change with increasing both model resolution as well as observations requires further investigation.

Code and data availability. Data from ERA5 (Hersbach et al., 2020) are available at <https://doi.org/10.24381/cds.adbb2d47>. Cyclone tracks based on ERA5 data are openly available at <https://doi.org/10.11582/2024.00023>. The Python library dynlib (Spensberger, 2024) is available <https://doi.org/10.11582/2024.00023>.

Competing interests. The authors declare that they have no conflict of interest.

305 *Author contributions.* QY performed data analyses and prepared the paper. CS, LM and TS contributed to the interpretation of the results and to the writing of the paper

Acknowledgements. We thank the ECMWF for making the reanalysis data openly available. This study was supported by the Research Council of Norway (Norges Forskningsråd, NFR) through the BALMCAST project (NFR grant number 324081).



References

310 Balasubramanian, G. and Yau, M.: The effects of convection on a simulated marine cyclone, *Journal of Atmospheric Sciences*, 51, 2397–2417, 1994.

Baumgart, M., Riemer, M., Wirth, V., Teubler, F., and Lang, S. T.: Potential vorticity dynamics of forecast errors: A quantitative case study, *Monthly Weather Review*, 146, 1405–1425, 2018.

Baumgart, M., Ghinassi, P., Wirth, V., Selz, T., Craig, G. C., and Riemer, M.: Quantitative view on the processes governing the upscale error growth up to the planetary scale using a stochastic convection scheme, *Monthly Weather Review*, 147, 1713–1731, 2019.

315 Binder, H., Boettcher, M., Joos, H., and Wernli, H.: The role of warm conveyor belts for the intensification of extratropical cyclones in Northern Hemisphere winter, *Journal of the Atmospheric Sciences*, 73, 3997–4020, 2016.

Bosart, L. F.: The Presidents' Day snowstorm of 18–19 February 1979: A subsynoptic-scale event, *Monthly Weather Review*, 109, 1542–1566, 1981.

320 Browning, K.: The dry intrusion perspective of extra-tropical cyclone development, *Meteorological Applications*, 4, 317–324, 1997.

Browning, K.: The sting at the end of the tail: Damaging winds associated with extratropical cyclones, *Quarterly Journal of the Royal Meteorological Society: A journal of the atmospheric sciences, applied meteorology and physical oceanography*, 130, 375–399, 2004.

Browning, K. A.: Organization of clouds and precipitation in extratropical cyclones, in: *Extratropical cyclones: the Erik Palmén memorial volume*, pp. 129–153, Springer, 1990.

325 Catto, J. L. and Pfahl, S.: The importance of fronts for extreme precipitation, *Journal of Geophysical Research: Atmospheres*, 118, 10–791, 2013.

Catto, J. L. and Raveh-Rubin, S.: Climatology and dynamics of the link between dry intrusions and cold fronts during winter. Part I: global climatology, *Climate Dynamics*, 53, 1873–1892, 2019.

Catto, J. L., Shaffrey, L. C., and Hodges, K. I.: Can climate models capture the structure of extratropical cyclones?, *Journal of Climate*, 23, 330 1621–1635, 2010.

Clark, P. A. and Gray, S. L.: Sting jets in extratropical cyclones: a review, *Quarterly Journal of the Royal Meteorological Society*, 144, 943–969, 2018.

Davies, H. C. and Didone, M.: Diagnosis and dynamics of forecast error growth, *Monthly weather review*, 141, 2483–2501, 2013.

Dirren, S., Didone, M., and Davies, H.: Diagnosis of “forecast-analysis” differences of a weather prediction system, *Geophysical research letters*, 30, 2003.

335 Eliassen, A.: On the vertical circulation in frontal zones, *Geofys. publ.*, 24, 147–160, 1962.

Froude, L. S., Bengtsson, L., and Hodges, K. I.: The predictability of extratropical storm tracks and the sensitivity of their prediction to the observing system, *Monthly weather review*, 135, 315–333, 2007.

Geer, A., Ahlgrimm, M., Bechtold, P., Bonavita, M., Bormann, N., English, S., Fielding, M., Forbes, R., Hogan, R., Hólm, E., et al.: 340 Assimilating observations sensitive to cloud and precipitation, *European Centre for Medium-Range Weather Forecasts*, 2017.

Gentile, E. S. and Gray, S. L.: Attribution of observed extreme marine wind speeds and associated hazards to midlatitude cyclone conveyor belt jets near the British Isles, *International Journal of Climatology*, 43, 2735–2753, 2023.

Grams, C. M., Magnusson, L., and Madonna, E.: An atmospheric dynamics perspective on the amplification and propagation of forecast error in numerical weather prediction models: A case study, *Quarterly Journal of the Royal Meteorological Society*, 144, 2577–2591, 2018.



345 Gyakum, J. R.: On the evolution of the QE II storm. II: Dynamic and thermodynamic structure, *Monthly Weather Review*, 111, 1156–1173, 1983.

Harvey, B., Methven, J., Sanchez, C., and Schäfler, A.: Diabatic generation of negative potential vorticity and its impact on the North Atlantic jet stream, *Quarterly Journal of the Royal Meteorological Society*, 146, 1477–1497, 2020.

Hersbach, H., Bell, B., Berrisford, P., Hirahara, S., Horányi, A., Muñoz-Sabater, J., Nicolas, J., Peubey, C., Radu, R., Schepers, D., et al.: 350 The ERA5 global reanalysis, *Quarterly Journal of the Royal Meteorological Society*, 146, 1999–2049, 2020.

Holton, J. R. and Hakim, G. J.: *An introduction to dynamic meteorology*, vol. 88, Academic press, 2013.

Hoskins, B. J. and Hodges, K. I.: New perspectives on the Northern Hemisphere winter storm tracks, *Journal of the Atmospheric Sciences*, 59, 1041–1061, 2002.

355 Joos, H. and Forbes, R. M.: Impact of different IFS microphysics on a warm conveyor belt and the downstream flow evolution, *Quarterly Journal of the Royal Meteorological Society*, 142, 2727–2739, 2016.

Klocke, D. and Rodwell, M.: A comparison of two numerical weather prediction methods for diagnosing fast-physics errors in climate models, *Quarterly Journal of the Royal Meteorological Society*, 140, 517–524, 2014.

Lamberson, W. S., Torn, R. D., Bosart, L. F., and Magnusson, L.: Diagnosis of the source and evolution of medium-range forecast errors for extratropical cyclone Joachim, *Weather and Forecasting*, 31, 1197–1214, 2016.

360 Marcheggiani, A., Dacre, H., Spensberger, C., and Spengler, T.: Weather features drive free-tropospheric baroclinicity variability in the North Atlantic storm track, *Quarterly Journal of the Royal Meteorological Society*, p. e5061, 2025.

Martínez-Alvarado, O., Baker, L. H., Gray, S. L., Methven, J., and Plant, R. S.: Distinguishing the cold conveyor belt and sting jet airstreams in an intense extratropical cyclone, *Monthly Weather Review*, 142, 2571–2595, 2014a.

Martínez-Alvarado, O., Joos, H., Chagnon, J., Boettcher, M., Gray, S., Plant, R., Methven, J., and Wernli, H.: The dichotomous structure of 365 the warm conveyor belt, *Quarterly Journal of the Royal Meteorological Society*, 140, 1809–1824, 2014b.

Martínez-Alvarado, O., Madonna, E., Gray, S. L., and Joos, H.: A route to systematic error in forecasts of Rossby waves, *Quarterly Journal of the Royal Meteorological Society*, 142, 196–210, 2016.

Murray, R. J. and Simmonds, I.: A numerical scheme for tracking cyclone centres from digital data. Part I: Development and operation of the scheme, *Australian meteorological magazine*, 39, 155–166, 1991a.

370 Murray, R. J. and Simmonds, I.: A numerical scheme for tracking cyclone centres from digital data. Part II: Application to January and July general circulation model simulations, *Australian Meteorological Magazine*, 39, 167–180, 1991b.

Oertel, A., Boettcher, M., Joos, H., Sprenger, M., and Wernli, H.: Potential vorticity structure of embedded convection in a warm conveyor belt and its relevance for large-scale dynamics, *Weather and Climate Dynamics*, 1, 127–153, 2020.

Papritz, L. and Spengler, T.: Analysis of the slope of isentropic surfaces and its tendencies over the North Atlantic, *Quarterly Journal of the 375 Royal Meteorological Society*, 141, 3226–3238, 2015.

Pickl, M., Quinting, J. F., and Grams, C. M.: Warm conveyor belts as amplifiers of forecast uncertainty, *Quarterly Journal of the Royal Meteorological Society*, 149, 3064–3085, 2023.

Pinto, J. G., Karremann, M. K., Born, K., Della-Marta, P. M., and Klawar, M.: Loss potentials associated with European windstorms under future climate conditions, *Climate Research*, 54, 1–20, 2012.

380 Raveh-Rubin, S.: Dry intrusions: Lagrangian climatology and dynamical impact on the planetary boundary layer, *Journal of Climate*, 30, 6661–6682, 2017.



Raveh-Rubin, S., Quinting, J., Kirsch, B., Oertel, A., Ramos, A., Schaefer, A., and Grams, C.: The North Atlantic Waveguide, Dry Intrusion, and Downstream Impact Campaign (NAWDIC), Tech. rep., Copernicus Meetings, 2025.

Robertson, F. and Smith, P.: The impact of model moist processes on the energetics of extratropical cyclones, *Monthly Weather Review*, 111, 385 723–744, 1983.

Rodwell, M. and Palmer, T.: Using numerical weather prediction to assess climate models, *Quarterly Journal of the Royal Meteorological Society: A journal of the atmospheric sciences, applied meteorology and physical oceanography*, 133, 129–146, 2007.

Sánchez, C., Methven, J., Gray, S., and Cullen, M.: Linking rapid forecast error growth to diabatic processes, *Quarterly Journal of the Royal Meteorological Society*, 146, 3548–3569, 2020.

390 Sanders, F. and Hoskins, B. J.: Diagnosis of frontogenesis and frontolysis from thermodynamic and kinematic fields, *Weather and Forecasting*, 5, 197–206, 1990.

Sawyer, J. S.: The vertical circulation at meteorological fronts and its relation to frontogenesis, *Proceedings of the Royal Society of London. Series A. Mathematical and Physical Sciences*, 234, 346–362, 1956.

Schäfler, A., Krüger, K., Oertel, A., Quinting, J., and Raveh-Rubin, S.: Indication for biases in dry intrusions and the marine boundary layer 395 over the Azores in ECMWF short-term forecasts and analyses, *Geophysical Research Letters*, 51, e2024GL109 601, 2024.

Schultz, D. M.: Reexamining the cold conveyor belt, *Monthly Weather Review*, 129, 2205–2225, 2001.

Spensberger, C.: Dynlib: a library of diagnostics, feature detection algorithms, plotting and convenience functions for dynamic meteorology, <https://doi.org/10.5281/zenodo.10471187>, 2024.

Spensberger, C. and Marcheggiani, A.: ERA5 cyclone tracks, <https://doi.org/10.11582/2024.00023>, 2024.

400 Teubler, F. and Riemer, M.: Dynamics of Rossby wave packets in a quantitative potential vorticity–potential temperature framework, *Journal of the Atmospheric Sciences*, 73, 1063–1081, 2016.

Tsopouridis, L., Spengler, T., and Spensberger, C.: SST fronts along the Gulf Stream and Kuroshio affect the winter climatology primarily in the absence of cyclones, *Weather and Climate Dynamics Discussions*, 2020, 1–27, 2020.

405 Vaughan, G., Methven, J., Anderson, D., Antonescu, B., Baker, L., Baker, T., Ballard, S., Bower, K., Brown, P., Chagnon, J., et al.: Cloud banding and winds in intense European cyclones: Results from the DIAMET project, *Bulletin of the American Meteorological Society*, 96, 249–265, 2015.

Wernli, H.: A Lagrangian-based analysis of extratropical cyclones. II: A detailed case-study, *Quarterly Journal of the Royal Meteorological Society*, 123, 1677–1706, 1997.

410 Wernli, H. and Gray, S. L.: The importance of diabatic processes for the dynamics of synoptic-scale extratropical weather systems—a review, *Weather and Climate Dynamics*, 5, 1299–1408, 2024.

Wimmer, M., Rivière, G., Arbogast, P., Piriou, J.-M., Delanoë, J., Labadie, C., Cazenave, Q., and Pelon, J.: Diabatic processes modulating the vertical structure of the jet stream above the cold front of an extratropical cyclone: sensitivity to deep convection schemes, *Weather and Climate Dynamics*, 3, 863–882, 2022.

Xie, S. et al.: On the correspondence between short- and long-timescale systematic errors in CAM4/CAM5, *Journal of Climate*, 25, 7937–415 7955, 2012.

Yu, Q., Spensberger, C., Magnusson, L., and Spengler, T.: Forecast Errors Attributed to Synoptic Features, *Meteorological Applications*, 32, e70093, 2025.